

New Cage-Like Cerium Trihydride Stabilized at Ambient Conditions

Xin Li^{1,2}, Xiaoli Huang^{1*}, Wuhao Chen¹, Di Zhou¹, Hui Xie¹, Quan Zhuang¹, Defang Duan¹ & Tian Cui^{1,3*}

¹State Key Laboratory of Superhard Materials, College of Physics, Jilin University, Changchun 130012, ²Synergetic Extreme Condition User Facility, Jilin University, Changchun 130012, ³School of Physical Science and Technology, Ningbo University, Ningbo 315211

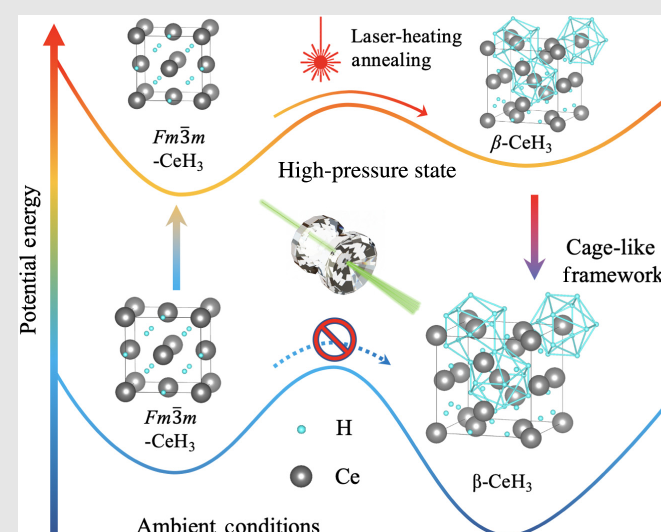
*Corresponding authors: huangxiaoli@jlu.edu.cn; cuitian@nbu.edu.cn

Cite this: *CCS Chem.* **2022**, 4, 825–831

DOI: [10.31635/ccschem.021.202100799](https://doi.org/10.31635/ccschem.021.202100799)

Metal hydrides, generally formed by high pressure combined with high-temperature conditions, have attracted substantial interest due to their promising high-energy density and high-temperature superconductivity. Although the synthesis and properties of these hydrides have been extensively studied, an important challenge is the lack of an efficient method to retain high-pressure phases. Herein, we have successfully quenched a high-pressure phase to ambient conditions with the precise control of different compression pathways. A new $\beta\text{-CeH}_3$ phase (space group $Pm\bar{3}n$) isostructural to $\beta\text{-UH}_3$ phase was synthesized by the reaction of Ce and H₂ above 33.0 GPa in a laser-heated diamond anvil cell. The $\beta\text{-CeH}_3$ phase has a cage-like framework structure that can be retained at ambient conditions. The electrical resistance as a function of temperature determines its metallic properties, but no superconductivity is observed in the current temperature range. Thermodynamic and dynamic calculations further prove the stability of $\beta\text{-CeH}_3$ at ambient

pressure. This work demonstrates that different synthesized paths will drive the formation of different products.



Keywords: high pressure, compression pathway, hydrides, crystal structure, X-ray diffraction

Introduction

Novel hydrides are currently the subject of great interest because some possess unique properties analogous to atomic metal hydrogen,^{1–5} and show promise as high-temperature superconductors and high-energy density materials. Remarkably, two main types of hydrides with intriguing high-temperature superconductivity have been uncovered by theoretical calculations and experimental methods, including covalent network

H₃S and clathrate structure LaH₁₀.^{6–12} H₃S has a body-centered cubic (bcc) lattice of S with H atoms located halfway between the S atoms, exhibiting covalent metallic characteristics. As the current record binary superconductor, LaH₁₀ has a clathrate-like structure of H with La atoms filling the clathrate cavities and has been described as an extended metallic hydrogen host structure stabilized by La atoms. These two discoveries open the door to achieving room-temperature superconductivity in compressed hydrogen-rich

DOI: [10.31635/ccschem.021.202100799](https://doi.org/10.31635/ccschem.021.202100799)

Corrected Citation: *CCS Chem.* **2022**, 4, 825–831

Previous Citation: *CCS Chem.* **2021**, 3, 1011–1017

Link to VoR: <https://doi.org/10.31635/ccschem.021.202100799>

materials and bring new interest in the manipulation of novel hydrogen-rich materials.

By tailoring intrinsic parameters, such as chemical composition, dimensionality engineering, and geometric size of the sample features, new materials can be obtained during synthesis and processing. Another possibility is to induce changes in the material through external parameters, such as temperature, pressure, epitaxial strain, or electric and magnetic fields. In particular, pressure can provide a different route for the synthesis of new materials and manipulation of novel physical properties. High pressure promotes the formation of novel hydrides with unusually high hydrogen-to-metal ratios. Upon compression, the chemical potential of hydrogen steeply increases and then hydrogen reacts with metals to form metal hydrides. Until recently, a series of results combining theory with experiment show that unconventional superhydrides with high hydrogen content can be formed at high pressures. In these superhydrides, one category is metallic hydrides formed by heavier elements, such as LaH_{10} ,¹³ CeH_9 ,¹⁴ PrH_9 ,¹⁵ NdH_9 ,¹⁶ ThH_9 ,¹⁷ UH_8 , and UH_9 ,¹⁸ and the others are molecular hydrides formed by lighter elements, such as LiH_6 ¹⁹ and NaH_7 .²⁰ Unfortunately, all of these superhydrides are stable only under high pressures and none of them can be quenched down to ambient conditions. Moreover, since most of the superhydrides have been synthesized at megabar pressures, such harsh conditions bring great difficulties to the experimental synthesis and largely

limit deeper research and further application of those novel hydrides.

Particularly, in these hydrides, LaH_{10} with the record superconducting T_c in binary hydrides is benefited by its clathrate structure with a large number of hydrogen ligands in the unit cell and larger strength of the electron-phonon interaction. Therefore, how to synthesize new hydrides with a clathrate structure under relatively mild conditions or stabilize them to nearly atmospheric conditions is urgently needed in this field of work. Following our recently published work on the Ce-H system,¹⁴ we are going to pursue new cerium hydrides by different compression pathways. In this work, we have successfully discovered the emergence of a new cage-like phase $\beta\text{-UH}_3\text{-CeH}_3$ (referred to as $\beta\text{-CeH}_3$), which is stable to at least 67 GPa upon compression, moreover, $\beta\text{-CeH}_3$ could be retained at ambient conditions.

Results

We have chosen elemental Ce and excess hydrogen as the reactants to guarantee the formation of novel cerium hydrides, which is similar to our previous work.¹⁴ After hydrogen loading into a diamond anvil cell (DAC) at 3.5 GPa, the synthesized hydride is identified as the known $Fm\bar{3}m\text{-CeH}_3$ (Figures 1a and 1b). Refinement of $Fm\bar{3}m\text{-CeH}_3$ gives a lattice constant of $a = 5.5093(5)$ Å, which is consistent with our previous experimental results.¹⁴ Upon further compression to 33 GPa, moderate

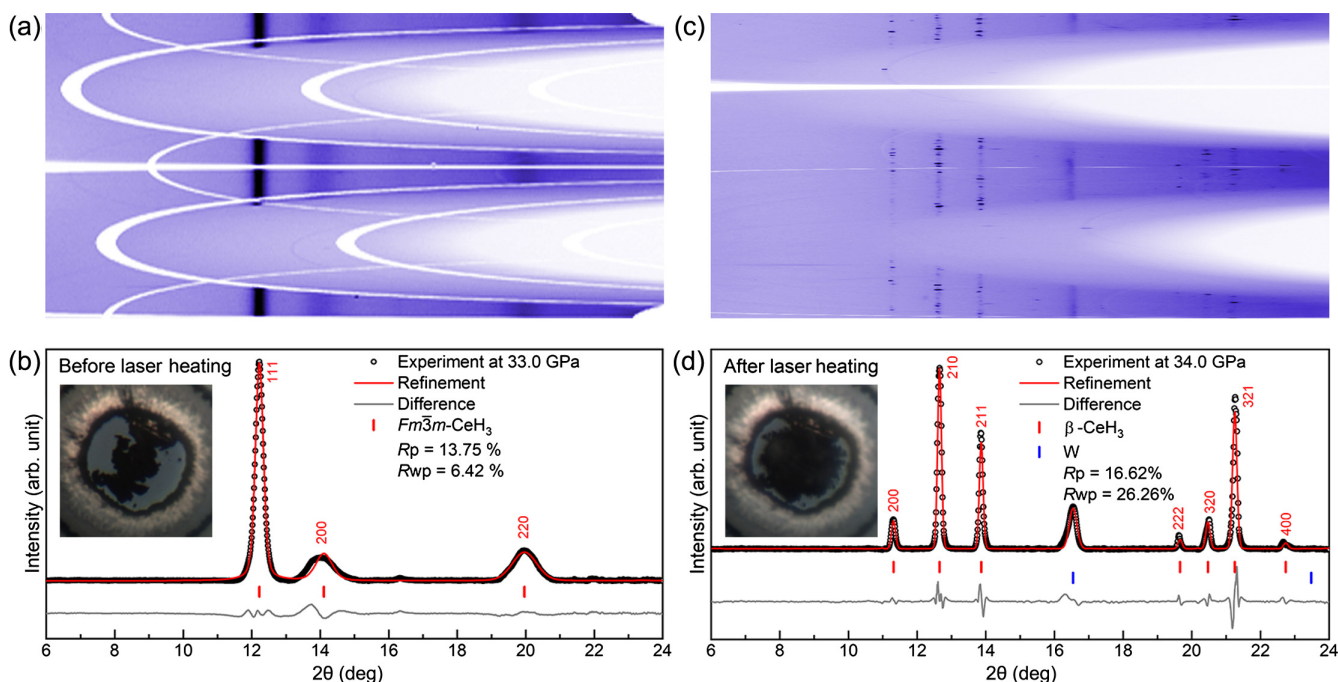


Figure 1 | (a) Unrolled recorded XRD image and (b) results of Rietveld refinement for $Fm\bar{3}m\text{-CeH}_3$ before laser heating at 33 GPa. (c) Unrolled recorded XRD image and (d) results of Rietveld refinement for $\beta\text{-CeH}_3$ after laser heating at 34 GPa. Insets of (b and d) show the sample chamber before and after laser heating, respectively.

DOI: 10.31635/ccschem.021.202100799

Corrected Citation: CCS Chem. 2022, 4, 825–831

Previous Citation: CCS Chem. 2021, 3, 1011–1017

Link to VoR: <https://doi.org/10.31635/ccschem.021.202100799>

laser heating was performed in DAC and the maximum heating temperature was about 1500 K. After laser heating, results reveal significant expansion in sample volumes and dramatic changes in X-ray diffraction (XRD) patterns, as shown in Figures 1c and 1d. Obvious new XRD peaks indicate the formation of a new cerium hydride after high-temperature annealing. All new peaks for this phase can be unambiguously indexed to a cubic lattice using Materials Studio software.²¹ The subsequent Rietveld refinement of the XRD pattern yields the symmetry $Pm\bar{3}n$ with $a = 6.2895(3)$ Å and Ce sublattice with Wyckoff positions 2a (0, 0, 0) and 6c (0.25, 0, 0.5) (Figure 1d). This new phase is referred to as β -CeH₃. We have performed five experimental runs of DACs (Supporting Information Table S1). Upon further compression (Run 1), XRD peaks broaden and weaken normally and the β -CeH₃ phase remains stable up to 69.4 GPa (Supporting Information Figure S1). Upon decompression to ambient pressure (Run 2), the synthesized β -CeH₃ is stable at ambient conditions (Figures 2a and 2b). To investigate the stability of β -CeH₃ against air, we have conducted experimental Run 3, where the detailed experimental setup can be found in the Supporting Information. The synthesized sample is exposed to the air and XRD patterns were collected for a specified duration, as is displayed in Figure 2c and Supporting Information

Figure S2. These data show that β -CeH₃ has good stability in air.

To give further evidence and determine the hydrogen content, we have also explored the equation of state (EOS) of the β -CeH₃ phase during compression and decompression routes. Figure 3a plots the pressure–volume (P – V) data collected from refinement results in both routes and Supporting Information Figure S3 plots P – V data with error bars. The P – V data are fitted by third-order Birch–Murnaghan (BM) EOS,²² yielding the ambient pressure volume $V_0 = 42.7$ (0.5) Å³, bulk modulus $K_0 = 62$ (4) GPa, and its pressure derivative $K_0' = 4$ (fixed). The volume expansion is crucial to estimate the hydrogen content of this cubic phase, as reported in previous work.¹⁴ At 34 GPa, $V(\text{CeH}_x) = 31.1$ Å³/formula, $V(\text{Ce}) = 18.6$ Å³/formula,²³ and $V(\text{H}_2) = 7.22$ Å³/formula.²⁴ Volume expansion is $V(\text{CeH}_x) - V(\text{Ce}) = 12.5$ Å³, thus the H content x is estimated to be about ~3. Besides considering that the volume of the high-pressure phase is also close to $Fm\bar{3}n$ -CeH₃ of 31.5 Å³/formula, β -CeH₃ phase matches a H:Ce ratio of 3. However, this is not a final confirmation, the determination of stoichiometry is the result of the combination of theory and experiment, rather than only one aspect. First, XRD data give the possible symmetry and match the proposed structure, and then theoretical calculation help us to finally determine the crystal structure and stoichiometry through

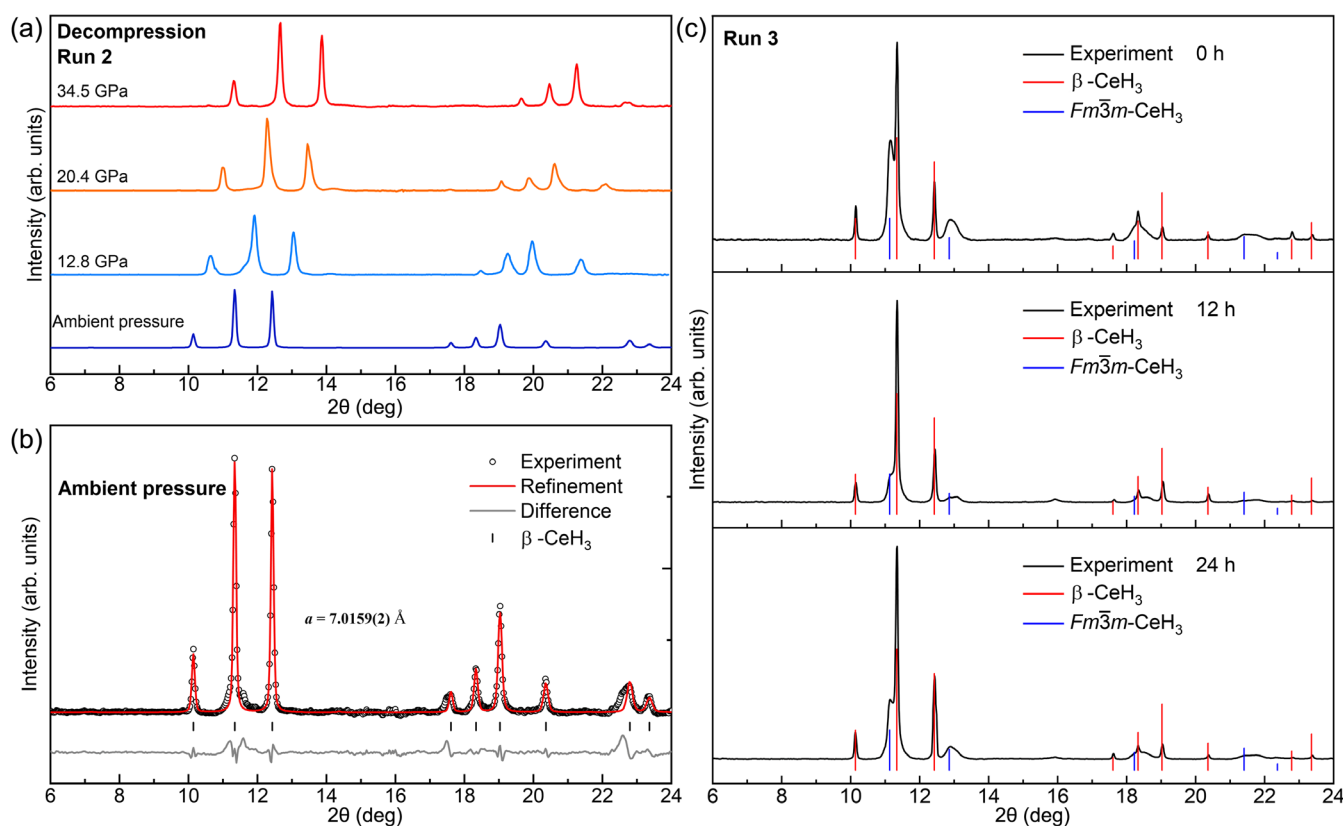


Figure 2 | (a) Selected typical XRD patterns upon decompression. (b) The Rietveld refinement results of β -CeH₃ at ambient conditions. (c) The XRD patterns of β -CeH₃ exposed to the air at different time durations.

DOI: 10.31635/ccschem.021.202100799

Corrected Citation: CCS Chem. 2022, 4, 825–831

Previous Citation: CCS Chem. 2021, 3, 1011–1017

Link to VoR: <https://doi.org/10.31635/ccschem.021.202100799>

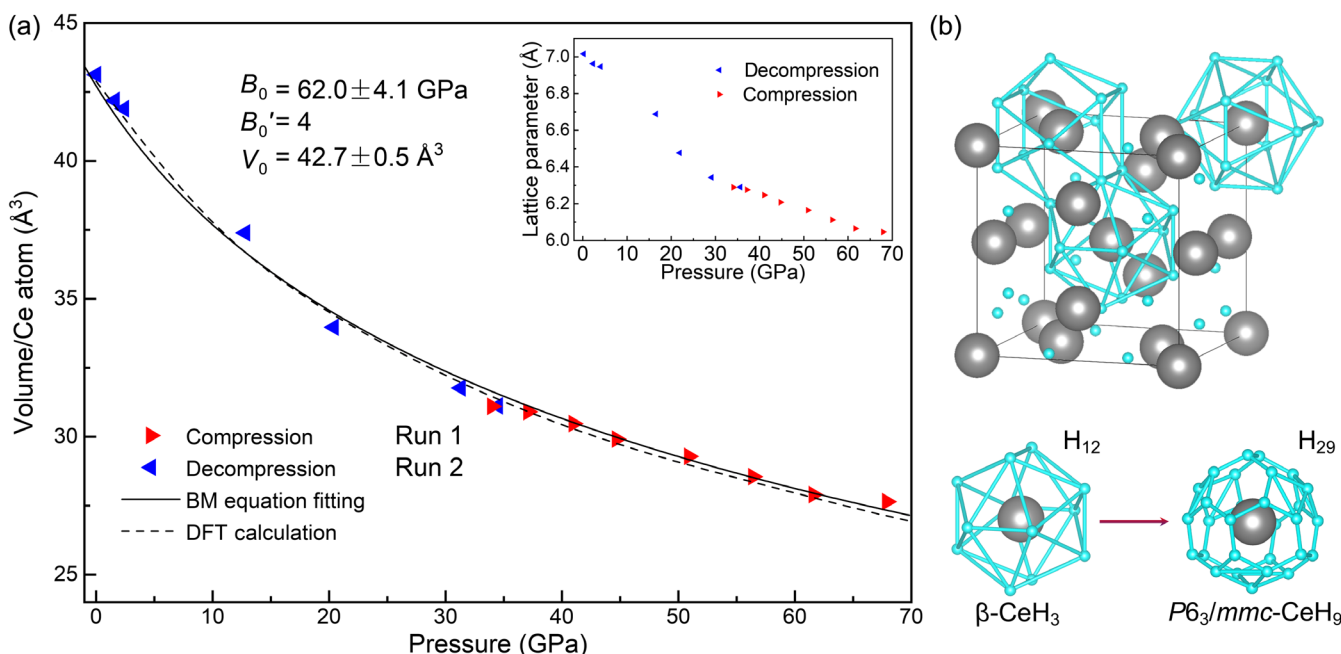


Figure 3 | (a) Volume per formula unit as a function of pressure for $\beta\text{-CeH}_3$. Red and blue triangle points indicate the compression and decompression processes, respectively. The solid line shows the fitted results by BM equation, where the dashed line represents calculated EOS of $\beta\text{-CeH}_3$. **(b)** Crystal structure with H_{12} cages of $\beta\text{-CeH}_3$ by contrast with H_{29} cage in $P6_3/mmc\text{-CeH}_9$. Large gray and small blue spheres represent Ce and H atoms, respectively. DFT, density functional theory.

calculated P - V relationships and thermodynamic and dynamic stabilities. Therefore, subsequent first-principle calculations are urgently required to determine the stoichiometry of this new hydride.

We have checked the five structures proposed in previous work,²⁵ but none could match the new cubic phase. Nevertheless, we found that the new XRD pattern of the high-pressure phase matches the preceding structure of $\beta\text{-UH}_3$,²⁶ and then we built the structure of the $\beta\text{-CeH}_3$ phase through atom substitution. The crystal structure is schematically shown in Figure 3b. Theoretical calculations were also carried out to check the thermodynamic and dynamic stability of $\beta\text{-CeH}_3$, which is shown to be thermodynamically stable through enthalpy calculations at ambient pressure (Figure 4a), while $Fm\bar{3}n\text{-CeH}_3$ is metastable relative to $\beta\text{-CeH}_3$. In our previous work,¹⁴ $Fm\bar{3}n\text{-CeH}_3$ would form $Pm\bar{3}n\text{-CeH}_3$ above 33 GPa without laser heating. The high-energy barrier prevents the formation of $\beta\text{-CeH}_3$ from $Fm\bar{3}n\text{-CeH}_3$, but laser heating treatment provides the extra energy to overcome the barrier for the transformation from $Fm\bar{3}n\text{-CeH}_3$ into $\beta\text{-CeH}_3$. The phonon dispersion curves show no imaginary frequency in the Brillouin zone, indicating the dynamic stability of $\beta\text{-CeH}_3$ at ambient pressure (Figure 4b and Supporting Information Figure S4).

In the $\beta\text{-CeH}_3$ structure, H atoms occupy the Wyckoff positions $24k$ (0, 0.1544, 0.6956), as determined through geometry optimization. Each Ce atom is linked with 12 H

atoms with Ce-H distance of 2.108–2.671 \AA , forming two kinds of H_{12} cage framework (Figure 3b). The shortest H-H distance is 2.108 \AA in the hydrogen sublattice of $\beta\text{-CeH}_3$. Based on the low hydrogen content and large distance between hydrogen atoms, there are no covalent interactions between hydrogen atoms in $\beta\text{-CeH}_3$. The calculated EOS is also in good agreement with experimental data, further proving the stoichiometric ratio and crystal structure of $\beta\text{-CeH}_3$. We also calculated the electronic properties for $\beta\text{-CeH}_3$ at 0 GPa (Figures 4c–4f). The band structure illustrates that $\beta\text{-CeH}_3$ exhibits apparently metallic character with a dense band around the Fermi level. Partial electronic densities of state (DOS) displays that Ce 4f and 5d states dominate the DOS and the contribution of the H s state is almost negligible at the Fermi level. Evidently, the electron localization function (ELF) map confirms the existence of isolated H atoms and differential charge density indicates the transfer of electrons from Ce to H atoms in $\beta\text{-CeH}_3$. Bader charges for H and Ce are –0.5435 and 1.6304, respectively.

We compared the crystal structure of $\beta\text{-CeH}_3$ with that of $Fm\bar{3}n\text{-CeH}_3$ and $Pm\bar{3}n\text{-CeH}_3$ (Supporting Information Table S2). $Fm\bar{3}n\text{-CeH}_3$ has a face-centered cubic (fcc) Ce lattice with four formula units and has similar volumes and trends of compression curves with $Pm\bar{3}n\text{-CeH}_3$ (Supporting Information Figure S5). We notice that $\beta\text{-CeH}_3$ and $Pm\bar{3}n\text{-CeH}_3$ have the same space group $Pm\bar{3}n$, but there are differences between them on the

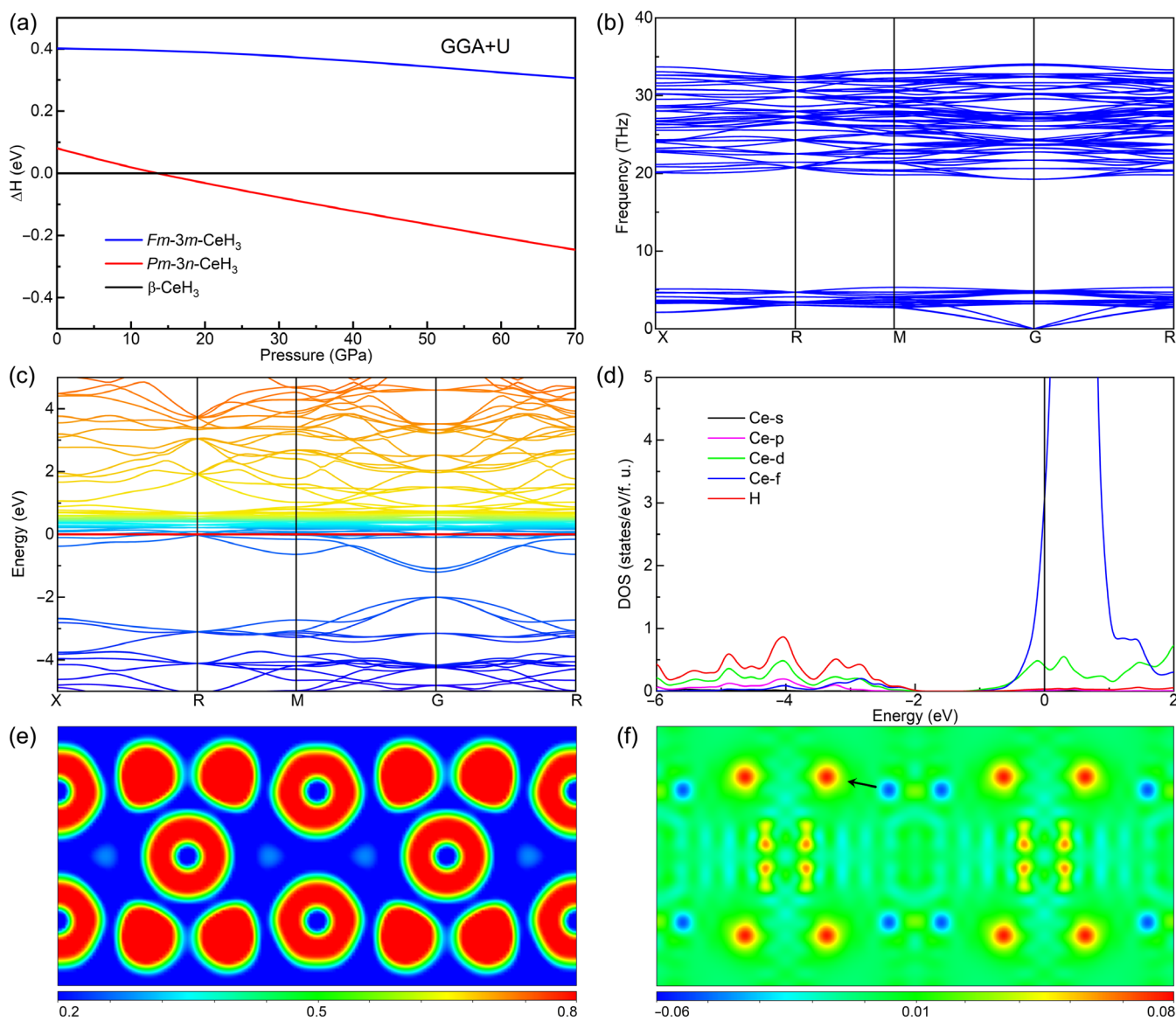


Figure 4 | (a) The calculated enthalpies as a function of pressure for $Fm\bar{3}m$ -CeH₃, $Pm\bar{3}n$ -CeH₃, and β -CeH₃ phases. The calculated (b) phonon dispersion, (c) band structure, (d) partial DOS, (e) ELF, and (f) differential charge density for β -CeH₃ at ambient pressure. GGA, generalized gradient approximation.

crystal structure and enthalpy. $Pm\bar{3}n$ -CeH₃ has a bcc Ce lattice with two formula units, while eight formula units in β -CeH₃. The calculated results present that β -CeH₃ has a lower enthalpy and is more stable than $Pm\bar{3}n$ -CeH₃ at ambient pressure. It is also the reason why β -CeH₃ forms under high-pressure and -temperature conditions and could be retained to ambient conditions.

To investigate the electronic properties of β -CeH₃, we performed high-pressure variable-temperature electrical resistance measurements on the target sample (Run 4). The scheme of the apparatus for four-probe electrical resistance measurement is shown in methods part. Supporting Information Figure S6 shows the measured electrical resistance of the sample as a function of temperature at 45 GPa. Characteristic metal behaviors, that

is, low resistance at low temperatures and nearly linear increase of resistivity with the temperature above 10 K, are observed at 45 GPa, but no obvious superconducting transition is found, so we did not perform further superconductivity calculations.

In a previous work,¹⁴ a series of new cerium polyhydrides were synthesized and presented the phase transformation sequence of $Fm\bar{3}n$ -CeH₃ \rightarrow $Pm\bar{3}n$ -CeH₃(CeH_{3+x}) \rightarrow I4/mmm-CeH₄ \rightarrow CeH_{9-δ} \rightarrow P6₃/mmc-CeH₉ through cold-compression engineering. However, this work reveals a transition: $Fm\bar{3}n$ -CeH₃ \rightarrow β -CeH₃ through high-temperature annealing (Figure 5 and Supporting Information Figure S7). Combining our reported results, this work further demonstrates the laser-heated sample is in favor of β -CeH₃, rather

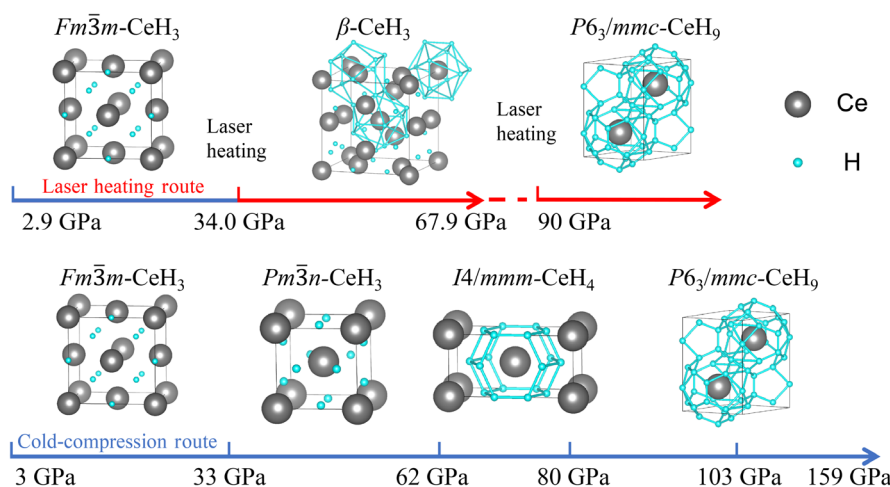


Figure 5 | Pressure stability ranges of different cerium hydrides between laser heating route (this work) and cold-compression route.¹⁴ The different routes affect the formation of products. Large gray and small blue spheres represent Ce and H atoms, respectively.

than $Pm\bar{3}n$ -CeH₃ or $I4/mmm$ -CeH₄. With subsequent pressure increases to 69.5 GPa, β -CeH₃ does not transform into other low-energy structures again because of the high-energy barrier. Laser heating treatment is performed on β -CeH₃ at higher pressure, more hydrogen atoms are absorbed into hydrogen framework, and β -CeH₃ could absorb hydrogen and become $P6_3/mmc$ -CeH₉.¹⁴ (Run 5, Supporting Information Figure S8). β -CeH₃ and $I4/mmm$ -CeH₄ have H₁₂ and H₁₈ cage-like framework, respectively, which are the precursors of $P6_3/mmc$ -CeH₉. This kind of cage-like framework is conducive to the formation of clathrate structure at high pressure. With increasing hydrogen content, the doping of Ce atoms stabilizes the hydrogen framework lattice, forming hydrogen cages in cerium hydrides.

In recent years, a large number of metal hydrides have been proposed through theoretical prediction methods under high pressure, but few hydrides have been synthesized in experiments. To obtain those metal hydrides, high pressure is an indispensable reaction condition and suitable temperature is provided to overcome the energy barrier. However, those high-pressure phases of hydrides can hardly be retained to ambient conditions. As described earlier, β -CeH₃ is the first sample to show that a synthesized preclathrate hydride become stable at ambient pressure, breaking through the classical understanding that those exciting hydrides cannot participate in future practical application. Further analysis shows that different compression routes point toward the various hydrides, which will consider an efficient strategy to control the products as well as the synthetic conditions. Besides, the joint high pressure and high temperature is a feasible alternate scheme to acquire hydrogen-rich compounds, which are stable at ambient conditions.

Conclusions

In this work, we have successfully synthesized a new hydride β -CeH₃ requiring a laser heating technique at 33 GPa. β -CeH₃ is considered as the precursor of clathrate $P6_3/mmc$ -CeH₉ with H₁₂ cage-like framework at lower pressure. β -CeH₃ could be quenched down to ambient conditions and experimentally determined as a typical metal. The theoretical calculation results show that this phase is both thermodynamically and dynamically stable at ambient pressure. The combination of high pressure and high temperature is demonstrated to be a means of acquiring a hydrogen-rich compound not achievable by conventional processing techniques. This work offers the possibility to stabilize the promising new hydrides to ambient conditions through controlled compression routes.

Supporting Information

Supporting Information is available and includes the detailed experimental procedures, Figures S1-S8, and Tables S1 and S2.

Conflict of Interest

The authors declare no competing financial interest.

Acknowledgments

In situ angle dispersive XRD of this work was performed at 4W2 HP-Station, Beijing Synchrotron Radiation Facility (BSRF) and 15U1 beamline, Shanghai Synchrotron Radiation Facility (SSRF). This work was supported by the

National Key R&D Program of China (no. 2018YFA0305900), National Natural Science Foundation of China (nos. 11974133, 516320025, and 51720105007), Program for Changjiang Scholars, Innovative Research Team in University (no. IRT_15R23), and China Postdoctoral Science Foundation (no. 2020M670835).

References

1. Ashcroft, N. W. Hydrogen Dominant Metallic Alloys: High Temperature Superconductors? *Phys. Rev. Lett.* **2004**, *92*, 4.
2. Sun, L.; Ruoff, A. L.; Zha, C.-S.; Stupian, G. High Pressure Studies on Silane to 210 GPa at 300 K: Optical Evidence of an Insulator-Semiconductor Transition. *J. Phys. Condens. Matter* **2006**, *18*, 8573–8580.
3. Feng, J.; Grochala, W.; Jaron, T.; Hoffmann, R.; Bergara, A.; Ashcroft, N. W. Structures and Potential Superconductivity in SiH₄ at High Pressure: En Route to “Metallic Hydrogen”. *Phys. Rev. Lett.* **2006**, *96*, 4.
4. Zurek, E.; Grochala, W. Predicting Crystal Structures and Properties of Matter Under Extreme Conditions via Quantum Mechanics: The Pressure Is On. *Phys. Chem. Chem. Phys.* **2015**, *17*, 2917–2934.
5. Chen, X. J.; Struzhkin, V. V.; Song, Y.; Goncharov, A. F.; Ahart, M.; Liu, Z. X.; Mao, H.; Hemley, R. J. Pressure-Induced Metallization of Silane. *Proc. Natl. Acad. Sci. U. S. A.* **2008**, *105*, 20–23.
6. Duan, D. F.; Liu, Y. X.; Tian, F. B.; Li, D.; Huang, X. L.; Zhao, Z. L.; Yu, H. Y.; Liu, B. B.; Tian, W. J.; Cui, T. Pressure-Induced Metallization of Dense (H₂S)₂H₂ with High-T_c Superconductivity. *Sci. Rep.* **2014**, *4*, 6.
7. Drozdov, A. P.; Eremets, M. I.; Troyan, I. A.; Ksenofontov, V.; Shylin, S. I. Conventional Superconductivity at 203 Kelvin at High Pressures in the Sulfur Hydride System. *Nature* **2015**, *525*, 73–76.
8. Einaga, M.; Sakata, M.; Ishikawa, T.; Shimizu, K.; Eremets, M. I.; Drozdov, A. P.; Troyan, I. A.; Hirao, N.; Ohishi, Y. Crystal Structure of the Superconducting Phase of Sulfur Hydride. *Nat. Phys.* **2016**, *12*, 835–838.
9. Liu, H. Y.; Naumov, I. I.; Hoffmann, R.; Ashcroft, N. W.; Hemley, R. J. Potential High-T_c Superconducting Lanthanum and Yttrium Hydrides at High Pressure. *Proc. Natl. Acad. Sci. U. S. A.* **2017**, *114*, 6990–6995.
10. Drozdov, A. P.; Kong, P. P.; Minkov, V. S.; Besedin, S. P.; Kuzovnikov, M. A.; Mozaffari, S.; Balicas, L.; Balakirev, F. F.; Graf, D. E.; Prakapenka, V. B.; Greenberg, E.; Knyazev, D. A.; Tkacz, M.; Eremets, M. I. Superconductivity at 250 K in Lanthanum Hydride Under High Pressures. *Nature* **2019**, *569*, 528.
11. Somayazulu, M.; Ahart, M.; Mishra, A. K.; Geballe, Z. M.; Baldini, M.; Meng, Y.; Struzhkin, V. V.; Hemley, R. J. Evidence for Superconductivity above 260 K in Lanthanum Superhydride at Megabar Pressures. *Phys. Rev. Lett.* **2019**, *122*, 027001.
12. Wang, H.; Tse, J. S.; Tanaka, K.; Itaya, T.; Ma, Y. M. Superconductive Soda-Like Clathrate Calcium Hydride at High Pressures. *Proc. Natl. Acad. Sci. U. S. A.* **2012**, *109*, 6463–6466.
13. Geballe, Z. M.; Liu, H. Y.; Mishra, A. K.; Ahart, M.; Somayazulu, M.; Meng, Y.; Baldini, M.; Hemley, R. J. Synthesis and Stability of Lanthanum Superhydrides. *Angew. Chem. Int. Ed.* **2018**, *57*, 688–692.
14. Li, X.; Huang, X. L.; Duan, D. F.; Pickard, C. J.; Zhou, D.; Xie, H.; Zhuang, Q.; Huang, Y. P.; Zhou, Q.; Liu, B. B.; Cui, T. Polyhydride CeH₉ with an Atomic-Like Hydrogen Clathrate Structure. *Nat. Commun.* **2019**, *10*, 7.
15. Zhou, D.; Semenok, D.; Duan, D. F.; Xie, H.; Huang, X. L.; Chen, W. H.; Li, X.; Liu, B. B.; Oganov, A. R.; Cui, T. Superconducting Praseodymium Superhydrides. *Sci. Adv.* **2020**, *6*, 8.
16. Zhou, D.; Semenok, D. V.; Xie, H.; Huang, X. L.; Duan, D. F.; Aperis, A.; Oppeneer, P. M.; Galasso, M.; Kartsev, A. I.; Kvashnin, A. G.; Oganov, A. R.; Cui, T. High-Pressure Synthesis of Magnetic Neodymium Polyhydrides. *J. Am. Chem. Soc.* **2020**, *142*, 2803–2811.
17. Semenok, D. V.; Kvashnin, A. G.; Ivanova, A. G.; Svitlyk, V.; Fominski, V. Y.; Sadakov, A. V.; Sobolevskiy, O. A.; Pudalov, V. M.; Troyan, I. A.; Oganov, A. R. Superconductivity at 161 K in Thorium Hydride ThH₁₀: Synthesis and Properties. *Mater. Today* **2020**, *33*, 36–44.
18. Kruglov, I. A.; Kvashnin, A. G.; Goncharov, A. F.; Oganov, A. R.; Lobanov, S. S.; Holtgrewe, N.; Jiang, S.; Prakapenka, V. B.; Greenberg, E.; Yanilkin, A. V. Uranium Polyhydrides at Moderate Pressures: Prediction, Synthesis, and Expected Superconductivity. *Sci. Adv.* **2018**, *4*, eaat9776.
19. Zurek, E.; Hoffmann, R.; Ashcroft, N. W.; Oganov, A. R.; Lyakhov, A. O. A Little Bit of Lithium Does a Lot for Hydrogen. *Proc. Natl. Acad. Sci. U. S. A.* **2009**, *106*, 17640–17643.
20. Struzhkin, V. V.; Kim, D. Y.; Stavrou, E.; Muramatsu, T.; Mao, H. K.; Pickard, C. J.; Needs, R. J.; Prakapenka, V. B.; Goncharov, A. F. Synthesis of Sodium Polyhydrides at High Pressures. *Nat. Commun.* **2016**, *7*, 8.
21. Young, R. The Rietveld Method. *Int. Union Crystallogr.* **1993**, *5*, 1–38.
22. Birch, F. The Effect of Pressure Upon the Elastic Parameters of Isotropic Solids, According to Murnaghan’s Theory of Finite Strain. *J. Appl. Phys.* **1938**, *9*, 279–288.
23. Vohra, Y. K.; Beaver, S. L.; Akella, J.; Ruddle, C. A.; Weir, S. T. Ultrapressure Equation of State of Cerium Metal to 208 GPa. *J. Appl. Phys.* **1999**, *85*, 2451–2453.
24. Loubeyre, P.; LeToullec, R.; Hausermann, D.; Hanfland, M.; Hemley, R. J.; Mao, H.; Finger, L. W. X-Ray Diffraction and Equation of State of Hydrogen at Megabar Pressures. *Nature* **1996**, *383*, 702–704.
25. Peng, F.; Sun, Y.; Pickard, C. J.; Needs, R. J.; Wu, Q.; Ma, Y. M. Hydrogen Clathrate Structures in Rare Earth Hydrides at High Pressures: Possible Route to Room-Temperature Superconductivity. *Phys. Rev. Lett.* **2017**, *119*, 6.
26. Halevy, I.; Salhov, S.; Zalkind, S.; Brill, M.; Yaar, I. High Pressure Study of β-UH₃ Crystallographic and Electronic Structure. *J. Alloy. Compd.* **2004**, *370*, 59–64.